PAPER

Check for updates

Two-dimensional eclipsed arrangement hybrid perovskites for tunable energy level alignments and photovoltaics†

Zhenyu Wang, [ID] [abc] Alex M. Ganose, [ID] [bcd] Chunming Niu[a] and David O. Scanlon [ID] *[bcd]

Excellent long-term durability and moisture tolerance, low cost synthesis routes, and the possibility of flexible tuning of electronic properties have meant that the two-dimensional (2D) hybrid halide perovskites have recently attracted much attention, and have been successfully used as light absorbers in efficient photovoltaic devices. 2D hybrid halides perovskites which feature long chain alkylammonium cations, however, are generally suggested for light emitting diode (LED) applications, due to their strong photoluminescence (PL), but none have been applied thus far for photovoltaic (PV) applications. Additionally, it has been shown that luminescence quenching occurs in the Pb-based analogues, $(AEQT)PbX_4$ (X = Cl, Br, I), however, energy transfer and charge separation between organic and inorganic components of the structures are still not fully understood. Herein, we investigate the geometrical, electronic and optical properties of the semiconducting 2D perovskites $(AEQT)BX_4$ (B = Pb, Sn; X = Cl, Br, I), using relativistic hybrid density functional theory calculations. We demonstrate that unlike the traditional 2D perovskites, the choice of the organic ammonium cation has a considerable effect on the carrier transport properties. Our calculations reveal that optical transitions between the organic and inorganic components is disallowed. The electronic structures of the series are flexibly tailored by different halides and metal cations, with band gaps ranging from 2.06 to 2.68 eV. Energy level alignments greatly hinder the electron–hole recombination in $(AEQT)PbCl_4$, $(AEQT)PbBr_4$, $(AEQT)PbI_4$ and $(AEQT)SnBr_4$, and thereby should enhance their PL efficiencies. With a moderate fundamental band gap (2.06 eV) and strong direct valence band to conduction band transition, $(AEQT)SnI_4$ is the only composition that shows intense and broad optical absorption, and as expected displays a high spectroscopic limited maximum efficiency (SLME) of 20.8%. Our results indicate the $(AEQT)SnI_4$ is a stable and efficient light-absorbing material for application as a top absorber of the tandem solar cell.

Introduction

Organic–inorganic lead halide perovskites have emerged as remarkable photovoltaic absorber materials in recent years.[1–6] To date, polycrystalline thin-film perovskite photovoltaic devices have reached power conversion efficiencies of 23.7%,[7] largely exceeding most of emerging PV devices, including

quantum dot cells, organic tandem cells, dye-sensitized solar cells.[8] Although three-dimensional (3D) organic–inorganic halide perovskite solar cells have experienced tremendous development in the past few decades, the involvement of toxic lead and long-term instability are preventing large scale commercialisation.[9–13]

Two-dimensional (2D) hybrid halide perovskites, a subclass of the organic–inorganic perovskites, were first synthesised by Mitzi *et al.* in 1994.[14] In 2014, Smith *et al.* reported that 2D perovskites display more resistance to moisture than their 3D counterparts,[15] opening a new path in the investigation of solar cell absorbers. One route to addressing the problem of toxicity is to replace lead with the less toxic Sn and Ge cations.[16–18] With appealing environmental stability and less toxic components, the Ruddlesden–Popper 2D tin perovskites have been introduced in solar cell devices, however with limited success in terms of efficiencies.[15,18–21] So far, general improvements in perovskite

[a] *Xi'an Jiaotong University, Center of Nanomaterials for Renewable Energy, State Key Lab of Electrical Insulation and Power Equipment, School of Electrical Engineering, 99 Yanxiang Road, Xi'an 710054, China*

[b] *Department of Chemistry, University College London, 20 Gordon Street, London WC1H 0AJ, UK. E-mail: d.scanlon@ucl.ac.uk*

[c] *Thomas Young Centre, University College London, Gower Street, London WC1E 6BT, UK*

[d] *Diamond Light Source Ltd, Diamond House, Harwell Science and Innovation Campus, Didcot, Oxfordshire OX11 0DE, UK*

† Electronic supplementary information (ESI) available. See DOI: 10.1039/c9tc01325c

This journal is © The Royal Society of Chemistry 2019

J. Mater. Chem. C, 2019, **7**, 5139–5147 | 5139

solar cell efficiency have primarily achieved by better control over thin film morphology, the choice of solvent treatment, and manipulation of the stoichiometry or chemistry of halide precursors (BX_2 or MAX, B = divalent metal, MA = $CH_3NH_3^+$, X = Cl, Br, I).[22,23] In this way, power conversion efficiencies have risen to 15.4% during the past two years.[24] In general, the fundamental band gap is determined mostly by the composition of the inorganic layer, which provides an effective route to tune their electronic properties. With regard to the well-known 3D perovskite, MAPI ($CH_3NH_3PbI_3$), changing halide composition allows tuning of the band gap from 1.6 to 3.1 eV.[25,26] Alternatively, replacing metal cation allows tuning from 1.6 to 2.0 eV.[27,28]

Classified by the position of metal atoms (B) from one inorganic layer over those in the adjacent ones, the 2D hybrid perovskites are generally sorted into "staggered" (($R-NH_3)_2BX_4$) and "eclipsed" arrangement (($H_3N-R-NH_3)BX_4$) (Fig. S1, ESI†), where $R-NH_3^+$ is an aliphatic or single ring aromatic ammonium cation, B is a divalent metal, and X is a halogen.[29,30] They both have multi-quantum-well structures of which semiconducting inorganic perovskite-like sheets are alternatively arranged with dye organic layers. Due to the large exciton binding energies and excitonic oscillator strengths of the materials, both types of layered systems have efficient photoluminescence and electroluminescence.[29,31–33] Additionally, the perovskite-like framework in the alternating structure will reduce the quenching interactions between dye molecules, and therefore further improve the luminescence efficiency.[34] To our knowledge, "staggered" arrangement perovskites and their analogues generally consist of small organic moieties, and the corresponding conduction band maximum (CBM) valence band minimum (VBM) are derived from the inorganic component. Recent evidence suggests that most of "staggered" arrangement perovskites have strong absorption in the visible light region and can be applied in visible light harvesting applications. However, the studies of the "eclipsed" arrangement perovskites are limited to the Pb- or Ge-based systems and the majority concentrate on the luminescence properties instead of their photovoltaic capabilities.[34–36]

In 1999, Mitzi and co-workers synthesised a series of "eclipsed" arrangement layered materials, $(AEQT)PbX_4$ (AEQT = $H_3NC_2H_4C_{16}H_8S_4C_2H_4NH_3^{2+}$; X = Cl, Br, I), and found the offsets between the energy levels of organic and inorganic components from distinct layers, of which the organic cation could play a role in the determination of band gaps and carrier mobility.[33,34] Recent theoretical research into the electronic structure of the analogues of $(AEQT)PbX_4$ ($AE4TPbX_4$) has revealed that due to the quantum-well-like behaviour of layered perovskites, the states associated with inorganic and organic components are possibly spatially well-separated,[37] thereby allowing for an additional degree of electronic structure tuning and effectively impeding the electron–hole recombination.

To date, an understanding of the Sn-based analogues is missing, and a non-toxic 2D hybrid halide would be of huge interest to the materials community and PV industry which deserves further study. Flexibly tunable energy level alignments and restricted energy loss from electron–hole recombination could enable these materials to be solar absorbers with the potential for high PV efficiencies. Studying electron transfer between different components during the photoelectric effect would be of great significance to understand whether the unique behaviour will enhance the PV or carrier transport performance. With these in mind, in this study, we report the crystal structures, electronic properties and optical properties of three Pb-based and three Sn-based layered perovskites, $(AEQT)BX_4$ (B = Pb, Sn; X = Cl, Br, I), using relativistic hybrid density functional theory. We provide an insight into the band offset of these series, shed light on the transition possibility between the inorganic framework and organic components, and how the selection of organic molecules affects the PV performance. With the evaluation of the thin-film PV ability, we demonstrate that $(AEQT)SnI_4$ holds promise for PV applications.

Computational details

First-principles calculations were carried out using the Vienna *ab initio* simulation package (VASP),[38–41] with the scalar relativistic projector augmented-wave (PAW) pseudopotentials applied to describe the interactions between core and valence electrons.[42,43] The plane wave cutoff energy was set to 580 eV, and *k*-point meshes of Γ-centered $4 \times 4 \times 2$ were employed for the geometry optimisation, electronic structure and optical property calculations. These parameters enable the total energy of each system converge within 10 meV per atom.

Lattice relaxations were tested *via* using the Perdew–Burke–Ernzerhof functional[44] (PBE), with dispersion interactions included *via* Grimme's D3 dispersion correction[45] (PBE-D3), and the PBEsol functional,[46] a version of PBE revised for solids. Both functionals are generally able to accurately reproduce the structural parameters of layered materials and containing weak long-range forces.[18,47–50] During geometry optimisation, the atomic positions, lattice shape and cell volume were allowed to relax, and were considered converged when all forces totalled less than 0.02 eV $Å^{-1}$.

In order to obtain an accurate description of the electronic structure of our systems, hybrid density functional theory was employed. Herein, we used the Heyd–Scuseria–Ernzerhof (HSE) functional[51,52] incorporating 43% HF exact exchange and 100% of the correlation energy from PBE. This has been shown to reproduce the band gap of MAPI and $BASnI_4$ (($CH_3(CH_2)_3NH_3)_2SnI_4$),[18,53] and therefore we expect that it will perform well here. Explicit treatment of spin–orbit coupling (SOC) effects is considered in all electronic structure calculations, due to the relativistic effects present on the heavy elements Pb, Sn and I.[54–57] This combination of HSE43 + SOC was used for all band structure, density of states, optical absorption and charge density calculations. The high-frequency dielectric response was calculated from the optical transition matrix elements within the transversal approximation.[58,59] The ionic dielectric contribution was calculated using density functional perturbation theory (DFPT),[60] using the PBE-D3 functional. Atom-projected band structure diagrams were plotted used the sumo package.[69]

5140 | *J. Mater. Chem. C*, 2019, **7**, 5139–5147

This journal is © The Royal Society of Chemistry 2019

Discussion and results

Crystal structure

Fig. 1 displays the crystal structures of the series, where each of the inorganic layers consists of sheets of corner-sharing metal halide octahedra ($[BX_6]^{4-}$). The B site cation (Pb^{2+} or Sn^{2+}) is generally a divalent metal that can adopt an octahedral coordination. The inorganic layers are separated by a long-chain bipolar $AEQT^{2+}$ dye molecule cation, where the cation spans the distance between adjacent inorganic layers, with both sides of ammonium head ionically bonding to the halogens in the inorganic layers.

All geometry relaxations were started from the experimental structures or from modifying the existing structures by swapping elements in the same group of the periodic table. Although $(AEQT)PbCl_4$, $(AEQT)PbBr_4$ and $(AEQT)PbI_4$ have been synthesized, only $(AEQT)PbBr_4$ has been structurally characterised.[34] Additionally, none of the Sn-based analogues have been reported thus far. Thus, only $(AEQT)PbBr_4$ is optimized from its experimental structure,[34] while the rest of the series ($(AEQT)PbCl_4$, $(AEQT)PbI_4$, $(AEQT)SnCl_4$, $(AEQT)SnBr_4$, and $(AEQT)SnI_4$) were created based on the structure of $(AEQT)PbBr_4$ via replacing Pb with Sn, and Br with Cl or I. Both PBE-D3 and PBEsol were tested for the geometry relaxations. The optimized lattice constants and available experimental data on the $(AEQT)BX_4$ structures are given in Table 1. The results indicated PBE-D3 gives better agreement with experiment for $(AEQT)PbBr_4$, and therefore PBE-D3 has been used for all of the structural analysis employed for the rest of the calculations. As a general trend, the metal–halogen bond lengths increase down Group VIIA, as is expected.[61] As shown in Table 1, we also see an enlargement of lattice parameters a and b, going from chloride to bromide and then to iodide, which is in agreement with the variation of the halogen ionic radii.

It is worthwhile mentioning that we obtained a different symmetry of 2D perovskites (Cc) to those in a recent computational study ($P2_1/c$).[37] As compared with the recent study in the Table S1 (ESI†),[37] we found our structures showed slightly contracted lattice parameters and were lower in energy, indicating they are the ground state structures at the level of theory used in this study. These differences could result from the different methodology for the relaxation. Although both studies used the PBE functional with dispersion corrections, in our work we have employed Grimme's corrections, whereas in the work by Blum and co-workers, the Tkatchenko–Scheffler.[37]

To test the stability of $(AEQT)BX_4$ (B = Pb, Sn; X = Cl, Br, I) in respect of stable compounds, we have tested two decomposition routes:

$$(AEQT)BX_4 \rightarrow (AEQT)X_2 + BX_2, \qquad (1)$$

$$(AEQT)BX_4 \rightarrow (AEQT–2H) + BX_2 + 2HX, \qquad (2)$$
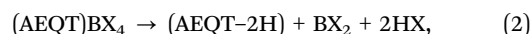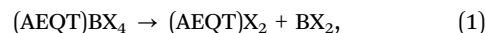
where AEQT–2H stands for the neutral molecule by removing two H atoms from the $AEQT^{2+}$ cation. The similar reaction pathways have been applied for estimation of the thermal stability of other hybrid perovskites, such as MAPI and its analogues.[50,62]

The enthalpies of decomposition for the pathways shown in eqn (1) and (2) are given as $\Delta_d H_1$ and $\Delta_d H_2$, respectively, and are provided in Table 1. Across all decomposition routes, all series showed positive enthalpies of decomposition, indicating that spontaneous decomposition is unfavourable.

Electronic properties

To assess the nature of the band gap in $(AEQT)BX_4$ (B = Pb, Sn; X = Cl, Br, I) series, and better understand the effects of the $AEQT^{2+}$ cation on the electronic structure of the layered perovskite, the band structures and the density of states (DOS) were calculated by HSE43 + SOC shown in Fig. S2 of the ESI.† The orbital-projected band structures are displayed in Fig. 2, and the fundamental band gaps and in-plane effective masses are listed in Table 2.

The fundamental band gaps of the Pb-based series increase from 2.06 eV (X = I) to 2.20 eV (X = Br), then to 2.45 eV (X = Cl), which shows the same trend in 3D lead halide perovskites.[25,26] Unlike the work by Blum and co-workers,[37] the Pb-based series we calculated were all indirect in nature, of which average energy difference between the direct and indirect band gaps is 0.04 eV across the series. In addition, the calculated band gaps were slightly larger by an average of 0.29 eV, though similar functionals were applied for geometry optimization and electronic property calculations. It is expected that these differences result from the different relaxed structures obtained by the different methodologies.[37] Both studies, however, found that the CBM of Pb-based series were composed of the p orbital of Pb and halogens, and their VBM originated from the $AEQT^{2+}$ cations. This induces the small electron effective mass ($< 0.5\ m_0$) and heavy hole effective mass ($> 27\ m_0$).

In terms of the Sn-based systems, the fundamental band gaps increase from 2.06 (X = I) to 2.67 (X = Cl) eV, and although indirect, they are only slightly indirect, with the direct band gaps only a maximum of 0.1 eV higher in energy across all cases. The frontier orbitals of the Sn-based series are derived from different components. The CBMs in $(AEQT)SnCl_4$ and $(AEQT)SnBr_4$
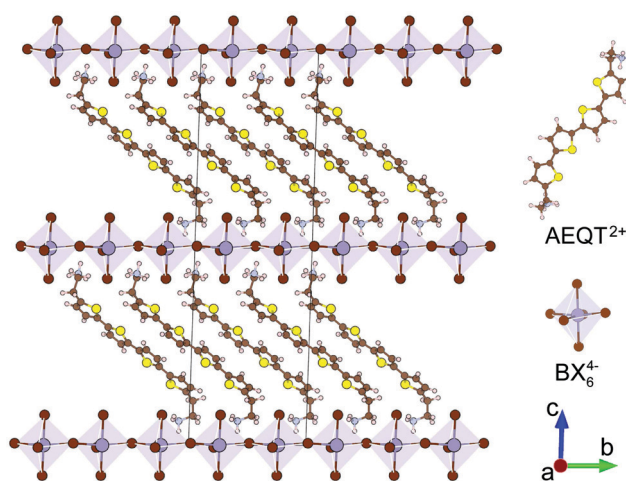

Fig. 1 Conventional cell of the layered perovskite series, $(AEQT)BX_4$ (B = Pb, Sn; X = Cl, Br, I).

This journal is © The Royal Society of Chemistry 2019

J. Mater. Chem. C, 2019, 7, 5139–5147 | 5141

Table 1 Lattice parameters of (AEQT)BX$_4$ (B = Pb, Sn; X = Cl, Br, I) conventional cells, calculated using the PBE functional with Grimme's D3 dispersion correction (PBE-D3), in comparison with PBEsol functional and experiment. Lattice lengths given in Å and lattice angles given in °. Enthalpy of decomposition, $\Delta_d H$ given in eV, with respect to the pathways shown in eqn (1) and (2)

Compounds	Functional	a	b	c	α	β	γ	$\Delta_d H_1$	$\Delta_d H_2$
(AEQT)PbCl$_4$	PBE-D3	5.596	11.346	39.976	92.5	90.0	90.0	4.32	6.90
(AEQT)PbBr$_4$	PBE-D3	5.762	11.824	39.037	91.9	90.0	90.0	4.26	7.38
	PBEsol	5.751	11.864	40.104	93.2	90.0	90.0	—	—
	Ref. 34	5.842	11.573	39.741	92.4	90.0	90.0	—	—
(AEQT)PbI$_4$	PBE-D3	6.054	12.589	38.072	92.2	90.0	90.0	3.81	7.19
(AEQT)SnCl$_4$	PBE-D3	5.677	11.175	39.803	92.8	90.0	90.0	4.34	6.93
(AEQT)SnBr$_4$	PBE-D3	5.847	11.608	38.989	91.9	90.0	90.0	4.28	7.40
(AEQT)SnI$_4$	PBE-D3	6.087	12.355	38.018	91.9	90.0	90.0	4.05	7.43

are determined by the molecular cation and inorganic framework, respectively, whereas their VBMs are both composed of the orbitals of AEQT^{2+} cation. Particularly, the conduction band edges of (AEQT)SnBr$_4$ nearly consists solely of AEQT^{2+} orbitals, because the energy difference between its CBM and lowest unoccupied molecular orbital (LUMO) of AEQT^{2+} cation is less than 20 meV. In contrast, like the majority of 3D perovskites, the frontier orbitals of (AEQT)SnBr$_4$ are composed of the inorganic components, of which CBM are derived from the Sn's p orbital, and VBM from Sn's s and I's p orbitals. For these reasons, (AEQT)SnI$_4$ exhibits dispersive VBM and CBM and relatively light effective masses (≈ 0.6 m_0). (AEQT)SnCl$_4$ and (AEQT)SnBr$_4$ share large hole effective mass (>15 m_0), while (AEQT)SnBr$_4$ possess a much smaller electron effective mass than (AEQT)SnCl$_4$. The atomic orbital contributions of the series at the VBM and CBM are further characterised by the electron density isosurfaces in Fig. S3 (ESI†).

As shown in Fig. 2, the highest occupied molecular orbital (HOMO) of AEQT^{2+} cation exhibits a very small variation amongst the series (<0.2 eV), and the maximum energy differences of their LUMO are 0.4 eV. Across the series, the organic HOMO–LUMO gaps exhibit a narrow range (2.66 to 2.80 eV), which is in agreement with 2.7 eV measured by the singlet transition of the organic chromophore in (AEQT)PbCl$_4$ *via* a photoluminescence measurement.[33] The minor variation of HOMO–LUMO gap is also confirmed by the recent theoretical study with energy of 2.2 to 2.4 eV.[37]

To illustrate the relative positions of band edges of organic and inorganic components from each series, each of their energy level is calculated with respect to the HOMO of AEQT^{2+} cations, respectively. It is found that their HOMO–LUMO gaps of AEQT^{2+} cation are similar, and thus their energy level schemes could be aligned together. To simplify the whole diagram, all separate schemes are merged relative to the same HOMO of AEQT^{2+} cation and depicted in Fig. 3. It is noted that this diagram does not indicate that the frontier orbitals of AEQT^{2+} cation with reference to the vacuum level stay the same across all series.

As displayed in the energy level diagram, the energy differences between the lead halide sheets in (AEQT)PbCl$_4$ and (AEQT)PbI$_4$ is 3.89 and 2.65 eV, respectively, which are close to the energy of the excitation band transition of the inorganic perovskite-like sheets (3.7 and 2.4 eV) measured by experiment.[33] Our calculations show excellent agreement with the experiment, and illustrate that except for (AEQT)SnCl$_4$ and (AEQT)SnI$_4$, the fundamental band

gaps (green numbers in Fig. 3) of the other series are smaller than the HOMO–LUMO gap of either inorganic or organic components.

Blum and co-workers recently sorted the hybrid organic–inorganic perovskites into four subgroups by comparing the positions in the band edges of the different components.[37] Using the same notation, we found three types across the series: Type Ia, where the low-energy electrons and holes are localized on the organic components, such as (AEQT)SnCl$_4$; Type Ib, where the low-energy electrons and holes are localized on the inorganic components, like (AEQT)SnI$_4$; Type IIb, where the electrons and holes are localized on the inorganic and organic components, respectively, for example, (AEQT)PbCl$_4$, (AEQT)PbBr$_4$, (AEQT)PbI$_4$ and (AEQT)SnBr$_4$. In the third group, due to the separation of electron and holes, the electron–hole recombination is expected to be reduced.

Optical properties

Fig. 4 shows the HSE43 + SOC calculated absorption spectra for (AEQT)BX$_4$ (B = Pb, Sn; X = Cl, Br, I). Uniquely, the trend of decreasing band gap as the halide ion increases is not observed in the optical absorption spectra. There are large differences between the fundamental direct band gaps and the adsorption edges in both the Pb-based and Sn-based series. We note large difference between the fundamental direct band gaps and the absorption edges in the Type IIb series, indicating the direct VB–CB optical transition from organic to inorganic component may be unfavourable. The optical transition matrix elements were calculated using the transversal approximation including explicit treatment of SOC effects.[63] Allowed and disallowed transitions were judged by the square of magnitude of matrix element, $|M|^2$.[64]

In all cases, the $|M|^2$ of the transition between the AEQT^{2+} cation and the perovskite-like framework is less than 10^{-3} eV^{-2} Å^{-2}, revealing this transition is unfavourable. This likely results from the limited orbital overlap of the organic and inorganic wavefunctions. In other words, only the transition from inorganic to inorganic components or from organic to organic components are allowed. Since the electrons and the holes are located separately across the alternative layers in the inorganic and organic hybrid components, in addition to the unfavourable transition between the two components, such unique energy level alignments therefore enable the electron–hole recombination to be suppressed among (AEQT)PbCl$_4$,
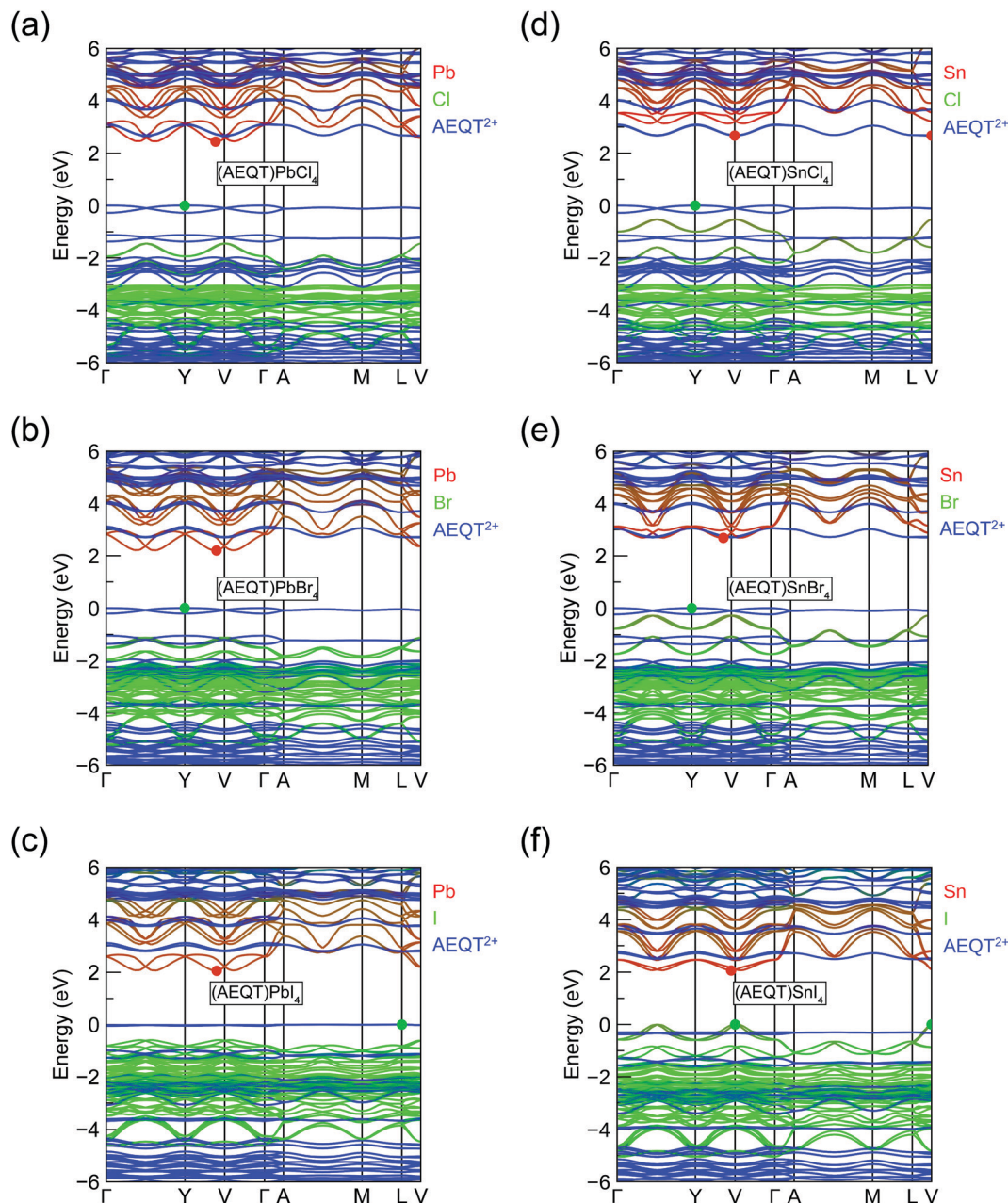
Fig. 2 HSE43 + SOC calculated atomic orbital projected band structures for the layered tin hybrid perovskites: (a) (AEQT)PbCl$_4$, (b) (AEQT)PbBr$_4$, (c) (AEQT)PbI$_4$, (d) (AEQT)SnCl$_4$, (e) (AEQT)SnBr$_4$ and (f) (AEQT)SnI$_4$. The valence band maximum is set to 0 eV. The red, green and blue lines stand for orbital from metal (Pb/Sn), halogen (Cl/Br/I), and AEQT^{2+}, respectively, of which line widths represent the orbital contribution. A green and red circles indicate the position of the valence band maximum and conduction band minimum.

(AEQT)PbBr$_4$, (AEQT)PbI$_4$ and (AEQT)SnBr$_4$, and find broad applications in the LED industry.

To evaluate the hypothetical photovoltaic performance of the series, a metric proposed by Yu and Zunger,[65] the spectroscopic limited maximum efficiency (SLME) with a thin film thickness of 0.5 μm, has been calculated and shown in Table 2. As (AEQT)SnI$_4$ exhibits strong and broad absorption in the visible light region, it possesses the highest SLME (20.8%). This is comparable to other Sn-based layered perovskites, such as (BA)$_2$(MA)Sn$_2$I$_7$ (BA = (CH$_3$(CH$_2$)$_3$NH$_2$)$_2^+$) (22.6%).[18] For the rest

of the series, the unfavourable inorganic–organic optical transition, coupled with large optical band gaps (>2.4 eV), results in very poor optical absorption in the visible light region and corresponding low SLMEs.

One of the distinct features of the 2D perovskites is their quantum-well-like structure, in which dielectric constant varies across the inorganic sheets ("wells") to the organic layers ("barriers") due to their different polarizability.[66,67] The dielectric constants for the full range of analogues are provided in Table 2. The dielectric constants in the direction parallel to

Table 2 Indirect (E_g^{Ind}) and direct (E_g^{Dir}) fundamental band gaps, dielectric constants (ε_r), and SLMEs of the series (AEQT)BX$_4$ (B = Pb, Sn; X = Cl, Br, I). Superscripts ∥ and ⊥ indicate properties parallel (in-plane) and perpendicular (out-of-plane) to the 2D perovskite sheets, respectively. Band gaps given in eV, effective masses given in units of electron rest mass (m_0), and SLME given in %

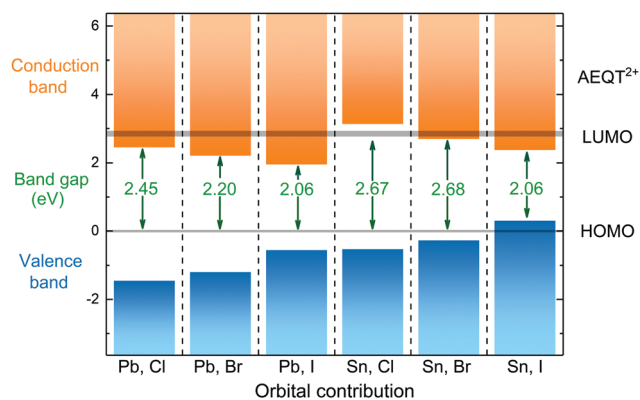| Compounds	E_g^{Ind}	E_g^{Dir}	$m_h^{\parallel}$	$m_e^{\parallel}$	$\varepsilon_r^{\parallel}$	$\varepsilon_r^{\perp}$	SLME^a
(AEQT)PbCl$_4$	2.45	2.50	27.30	0.47	4.84	3.34	9.5
(AEQT)PbBr$_4$	2.20	2.24	46.60	0.47	4.79	3.13	12.5
(AEQT)PbI$_4$	2.06	2.07	105.21	0.43	4.92	3.08	7.7
(AEQT)SnCl$_4$	2.67	2.77	15.45	1.38	10.29	4.37	7.9
(AEQT)SnBr$_4$	2.68	2.73	19.34	0.80	12.04	3.64	7.8
(AEQT)SnI$_4$	2.06	2.07	0.63	0.50	12.37	5.09	20.8

^{a} Thickness: 0.5 μm.

Fig. 3 Orbital contribution near the band edge of (AEQT)BX$_4$ (B = Pb, Sn; X = Cl, Br, I) series, where the HOMO of AEQT^{2+} is set to 0 eV. The LUMO and HOMO is represented by grey shadow, of which thickness indicate the energy range of the orbitals.
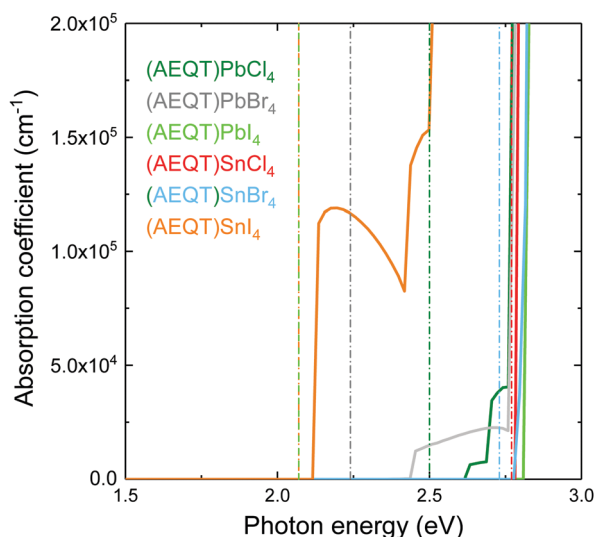

Fig. 4 Calculated optical absorption spectra for layered hybrid perovskites: (AEQT)PbCl$_4$, (AEQT)PbBr$_4$, (AEQT)PbI$_4$, (AEQT)SnCl$_4$, (AEQT)SnBr$_4$ and (AEQT)SnI$_4$, where the vertical dash lines are the corresponding fundamental direct band gaps.

the perovskite-like sheets ($\varepsilon_r^{\parallel}$) are larger than those in the direction perpendicular to the sheets ($\varepsilon_r^{\perp}$), which is in agreement with studies of other layered perovskite systems.[18,50] Both the in-plane and out-of-plane dielectric constants for Sn-based series are larger than those in the Pb-based ones, which can be explained by the larger Born effective charges of Sn-based series (Table S2, ESI†). Particularly, among both Pb- and Sn-based series, (AEQT)SnI$_4$ exhibit the largest dielectric constants with $\varepsilon_r^{\parallel}$ = 12.37 and $\varepsilon_r^{\perp}$ = 5.09, in which the in-plane one is comparable to (MA)$_2$Sn(SeCN)$_2$Cl$_2$ ($\varepsilon_r^{\parallel}$ = 11.7) while the out-of-plane one is comparable to (BA)$_2$SnI$_4$ ($\varepsilon_r^{\perp}$ = 4.5).[18,50] Furthermore, large dielectric constants are proposed to be an indicator of defect tolerance, and so these systems could be insensitive to lattice imperfections and can achieve a relatively high optoelectronic energy.[68]

Conclusions

In conclusion, we have demonstrated that the electronic properties of (AEQT)BX$_4$ (B = Pb, Sn; X = Cl, Br, I) can be tuned through incorporation of different halides and metal cations, with band gaps varying from 2.06–2.68 eV. The location of frontier orbitals varies according to the halide and metal. Such tunability of electronic properties, especially the energy level alignments of organic and inorganic components, opens up the possibility to theoretically tailor charge separation or recombination, which is important to suppress the PL quenching caused by electron–hole recombination. The unique energy alignments of (AEQT)PbCl$_4$, (AEQT)PbBr$_4$, (AEQT)PbI$_4$ and (AEQT)SnBr$_4$ may make them of use in the LED industry. The transition between the organic and inorganic components is confirmed to be unfavourable, resulting in poor absorption of light in the visible spectrum for most of the series. However, we identify a novel 2D perovskite material, (AEQT)SnI$_4$, in which the VBM and CBM are composed of contributions from the inorganic sheets. Due to its broad absorption in the visible light region, reasonably large dielectric constants and SLME of 20.8%, (AEQT)SnI$_4$ shows a promise as a potential solar absorber. (AEQT)SnI$_4$ thus presents an exciting prospect because of its earth abundance, and possible enhanced moisture stability and defect tolerance. Experimental verification of our computational predictions are welcomed.

Conflicts of interest

There are no conflicts to declare.

Acknowledgements

5144 | *J. Mater. Chem. C*, 2019, **7**, 5139–5147

This journal is © The Royal Society of Chemistry 2019

References

1 A. Kojima, K. Teshima, Y. Shirai and T. Miyasaka, Organo-metal halide perovskites as visible-light sensitizers for photovoltaic cells, *J. Am. Chem. Soc.*, 2009, **131**, 6050–6051.

2 H.-S. Kim, C.-R. Lee, J.-H. Im, K.-B. Lee, T. Moehl, A. Marchioro, S.-J. Moon, R. Humphry-Baker, J.-H. Yum, J. E. Moser, M. Grätzel and N.-G. Park, Lead iodide perovskite sensitized all-solid-state submicron thin film mesoscopic solar cell with efficiency exceeding 9%, *Sci. Rep.*, 2012, **2**, 591.

3 J. Burschka, N. Pellet, S.-J. Moon, R. Humphry-Baker, P. Gao, M. K. Nazeeruddin and M. Grätzel, Sequential deposition as a route to high-performance perovskite-sensitized solar cells, *Nature*, 2013, **499**, 316–319.

4 M. A. Green, A. Ho-Baillie and H. J. Snaith, The emergence of perovskite solar cells, *Nat. Photonics*, 2014, **8**, 506–514.

5 A. Polman, M. Knight, E. C. Garnett, B. Ehrler and W. C. Sinke, Photovoltaic materials: present efficiencies and future challenges, *Science*, 2016, **352**, aad4424.

6 W. S. Yang, B.-W. Park, E. H. Jung, N. J. Jeon, Y. C. Kim, D. U. Lee, S. S. Shin, J. Seo, E. K. Kim, J. H. Noh and S. I. Seok, Iodide management in formamidinium-lead-halide-based perovskite layers for efficient solar cells, *Science*, 2017, **356**, 1376–1379.

7 https://www.nrel.gov/pv/assets/pdfs/best-reserch-cell-efficiencies.pdf (Access 10 March 2019).

8 M. A. Green, Y. Hishikawa, W. Warta, E. D. Dunlop, D. H. Levi, J. Hohl-Ebinger and A. W. Ho-Baillie, Solar cell efficiency tables (version 50), *Prog. Photovoltaics*, 2017, **25**, 668–676.

9 G. Niu, X. Guo and L. Wang, Review of recent progress in chemical stability of perovskite solar cells, *J. Mater. Chem. A*, 2015, **3**, 8970–8980.

10 S. Ahmad, P. K. Kanaujia, H. J. Beeson, A. Abate, F. Deschler, D. Credgington, U. Steiner, G. V. Prakash and J. J. Baumberg, Strong Photocurrent from Two-Dimensional Excitons in Solution-processed Stacked Perovskite Semiconductor Sheets, *ACS Appl. Mater. Interfaces*, 2015, **7**, 25227–25236.

11 G. Nagabhushana, R. Shivaramaiah and A. Navrotsky, Direct calorimetric verification of thermodynamic instability of lead halide hybrid perovskites, *Proc. Natl. Acad. Sci. U. S. A.*, 2016, **113**, 7717–7721.

12 T. W. Kasel and C. H. Hendon, Electronic implications of organic nitrogen lone pairs in lead iodide perovskites, *J. Mater. Chem. C*, 2018, **6**, 4765–4768.

13 L. Meng, J. You and Y. Yang, Addressing the stability issue of perovskite solar cells for commercial applications, *Nat. Commun.*, 2018, **9**, 5265.

14 D. B. Mitzi, C. A. Feild, W. T. A. Harrison and A. M. Guloy, Conducting tin halides with a layered organic-based perovskite structure, *Nature*, 1994, **369**, 467–469.

15 I. C. Smith, E. T. Hoke, D. Solis-Ibarra, M. D. McGehee and H. I. Karunadasa, A Layered Hybrid Perovskite Solar-Cell Absorber with Enhanced Moisture Stability, *Angew. Chem., Int. Ed.*, 2014, **126**, 11414–11417.

16 D. H. Cao, C. C. Stoumpos, T. Yokoyama, J. L. Logsdon, T.-B. Song, O. K. Farha, M. R. Wasielewski, J. T. Hupp and M. G. Kanatzidis, Thin Films and Solar Cells Based on Semiconducting Two-Dimensional Ruddlesden–Popper $(CH_3(CH_2)_3NH_3)_2(CH_3NH_3)_{n-1}Sn_nI_{3n+1}$ Perovskites, *ACS Energy Lett.*, 2017, **2**, 982–990.

17 P. Cheng, T. Wu, J. Zhang, Y. Li, J. Liu, L. Jiang, X. Mao, R.-F. Lu, W.-Q. Deng and K. Han, $(C_6H_5C_2H_4NH_3)_2GeI_4$: A Layered Two-Dimensional Perovskite with Potential for Photovoltaic Applications, *J. Phys. Chem. Lett.*, 2017, **8**, 4402–4406.

18 Z. Wang, A. M. Ganose, C. Niu and D. O. Scanlon, First-principles insights into tin-based two dimensional hybrid halide perovskites for photovoltaics, *J. Mater. Chem. A*, 2018, **6**, 5652–5660.

19 D. H. Cao, C. C. Stoumpos, O. K. Farha, J. T. Hupp and M. G. Kanatzidis, 2D homologous perovskites as light-absorbing materials for solar cell applications, *J. Am. Chem. Soc.*, 2015, **137**, 7843–7850.

20 H. Tsai, *et al.*, High-efficiency two-dimensional Ruddlesden-Popper perovskite solar cells, *Nature*, 2016, **536**, 312–316.

21 L. N. Quan, M. Yuan, R. Comin, O. Voznyy, E. M. Beauregard, S. Hoogland, A. Buin, A. R. Kirmani, K. Zhao, A. Amassian, D. H. Kim and E. H. Sargent, Ligand-stabilized reduced-dimensionality perovskites, *J. Am. Chem. Soc.*, 2016, **138**, 2649–2655.

22 J. S. Manser, M. I. Saidaminov, J. A. Christians, O. M. Bakr and P. V. Kamat, Making and breaking of lead halide perovskites, *Acc. Chem. Res.*, 2016, **49**, 330–338.

23 Y. Hu, L. M. Spies, D. Alonso-Álvarez, P. Mocherla, H. Jones, J. Hanisch, T. Bein, P. R. F. Barnes and P. Docampo, Identifying and controlling phase purity in 2D hybrid perovskite thin films, *J. Mater. Chem. A*, 2018, **6**, 22215–22225.

24 A. M. Ganose, C. N. Savory and D. O. Scanlon, Beyond Methylammonium Lead Iodide: Prospects for the Emergent Field of ns^2 Containing Solar Absorbers, *Chem. Commun.*, 2017, **53**, 20–44.

25 A. Sadhanala, F. Deschler, T. H. Thomas, S. E. Dutton, K. C. Goedel, F. C. Hanusch, M. L. Lai, U. Steiner, T. Bein, P. Docampo, D. Cahen and R. H. Friend, Preparation of single-phase films of $CH_3NH_3Pb(I_{1-x}Br_x)_3$ with sharp optical band edges, *J. Phys. Chem. Lett.*, 2014, **5**, 2501–2505.

26 A. Sadhanala, S. Ahmad, B. Zhao, N. Giesbrecht, P. M. Pearce, F. Deschler, R. L. Z. Hoye, K. C. Goödel, T. Bein, P. Docampo, S. E. Dutton, M. F. L. De Volder and R. H. Friend, Blue-green color tunable solution processable

This journal is © The Royal Society of Chemistry 2019

J. Mater. Chem. C, 2019, **7**, 5139–5147 | 5145

organolead chloride–bromide mixed halide perovskites for optoelectronic applications, *Nano Lett.*, 2015, **15**, 6095–6101.

27 F. Hao, C. C. Stoumpos, D. H. Cao, R. P. Chang and M. G. Kanatzidis, Lead-free solid-state organic-inorganic halide perovskite solar cells, *Nat. Photonics*, 2014, **8**, 489–494.

28 T. Krishnamoorthy, H. Ding, C. Yan, W. L. Leong, T. Baikie, Z. Zhang, M. Sherburne, S. Li, M. Asta, N. Mathews and S. G. Mhaisalkar, Lead-free germanium iodide perovskite materials for photovoltaic applications, *J. Mater. Chem. A*, 2015, **3**, 23829–23832.

29 D. B. Mitzi, K. Chondroudis and C. R. Kagan, Organic-inorganic electronics, *IBM J. Res. Dev.*, 2001, **45**, 29–45.

30 D. B. Synthesis Mitzi, structure, and properties of organic-inorganic perovskites and related materials, *Prog. Inorg. Chem.*, 2007, 1–121.

31 M. Era, S. Morimoto, T. Tsutsui and S. Saito, Organic–inorganic heterostructure electroluminescent device using a layered perovskite semiconductor $(C_6H_5C_2H_4NH_3)_2PbI_4$, *Appl. Phys. Lett.*, 1994, **65**, 676–678.

32 D. B. Mitzi, Synthesis, Crystal Structure, and Optical and Thermal Properties of $(C_4H_9NH_3)_2MI_4$ (M = Ge, Sn, Pb), *Chem. Mater.*, 1996, **8**, 791–800.

33 D. B. Mitzi, K. Chondroudis and C. R. Kagan, Design, structure, and optical properties of organic–inorganic perovskites containing an oligothiophene chromophore, *Inorg. Chem.*, 1999, **38**, 6246–6256.

34 K. Chondroudis and D. B. Mitzi, Electroluminescence from an organic–inorganic perovskite incorporating a quaterthiophene dye within lead halide perovskite layers, *Chem. Mater.*, 1999, **11**, 3028–3030.

35 T. Ishihara, J. Takahashi and T. Goto, Exciton state in two-dimensional perovskite semiconductor $(C_{10}H_{21}NH_3)_2PbI_4$, *Solid State Commun.*, 1989, **69**, 933–936.

36 S. Ahmad and G. V. Prakash, Strong room-temperature ultraviolet to red excitons from inorganic organic-layered perovskites, $(R-NH_3)_2MX_4$ ($M = Pb^{2+}, Sn^{2+}, Hg^{2+}; X = I^-, Br^-$), *J. Nanophotonics*, 2014, **8**, 083892.

37 C. Liu, W. Huhn, K.-Z. Du, A. Vazquez-Mayagoitia, D. Dirkes, W. You, Y. Kanai, D. B. Mitzi and V. Blum, Tunable Semiconductors: Control over Carrier States and Excitations in Layered Hybrid Organic-Inorganic Perovskites, *Phys. Rev. Lett.*, 2018, **121**, 146401.

38 G. Kresse and J. Hafner, Ab initio molecular dynamics for liquid metals, *Phys. Rev. B: Condens. Matter Mater. Phys.*, 1993, **47**, 558.

39 G. Kresse and J. Hafner, Ab initio molecular-dynamics simulation of the liquid-metal-amorphous-semiconductor transition in germanium, *Phys. Rev. B: Condens. Matter Mater. Phys.*, 1994, **49**, 14251.

40 G. Kresse and J. Furthmüller, Efficient iterative schemes for ab initio total-energy calculations using a plane-wave basis set, *Phys. Rev. B: Condens. Matter Mater. Phys.*, 1996, **54**, 11169.

41 G. Kresse and J. Furthmüller, Efficiency of ab-initio total energy calculations for metals and semiconductors using a plane-wave basis set, *Comput. Mater. Sci.*, 1996, **6**, 15–50.

42 P. E. Blöchl, Projector augmented-wave method, *Phys. Rev. B: Condens. Matter Mater. Phys.*, 1994, **50**, 17953.

43 G. Kresse and D. Joubert, From ultrasoft pseudopotentials to the projector augmented-wave method, *Phys. Rev. B: Condens. Matter Mater. Phys.*, 1999, **59**, 1758.

44 J. P. Perdew, K. Burke and M. Ernzerhof, Generalized gradient approximation made simple, *Phys. Rev. Lett.*, 1996, **77**, 3865.

45 S. Grimme, Accurate description of van der Waals complexes by density functional theory including empirical corrections, *J. Comput. Chem.*, 2004, **25**, 1463–1473.

46 J. P. Perdew, A. Ruzsinszky, G. I. Csonka, O. A. Vydrov, G. E. Scuseria, L. A. Constantin, X. Zhou and K. Burke, Restoring the density-gradient expansion for exchange in solids and surfaces, *Phys. Rev. Lett.*, 2008, **100**, 136406.

47 F. Brivio, A. B. Walker and A. Walsh, Structural and Electronic Properties of Hybrid Perovskites for High-Efficiency Thin-Film Photovoltaics from First-Principles, *APL Mater.*, 2013, **1**, 042111.

48 K. T. Butler, J. M. Frost and A. Walsh, Band alignment of the hybrid halide perovskites $CH_3NH_3PbCl_3$, $CH_3NH_3PbBr_3$ and $CH_3NH_3PbI_3$, *Mater. Horiz.*, 2015, **2**, 228–231.

49 A. M. Ganose, K. T. Butler, A. Walsh and D. O. Scanlon, Relativistic electronic structure and band alignment of BiSI and BiSeI: candidate photovoltaic materials, *J. Mater. Chem. A*, 2016, **4**, 2060–2068.

50 A. M. Ganose, C. N. Savory and D. O. Scanlon, Electronic and defect properties of $(CH_3NH_3)_2Pb(SCN)_2I_2$ analogues for photovoltaic applications, *J. Mater. Chem. A*, 2017, **5**, 7845–7853.

51 J. Heyd, G. E. Scuseria and M. Ernzerhof, Hybrid functionals based on a screened Coulomb potential, *J. Chem. Phys.*, 2003, **118**, 8207–8215.

52 J. Heyd, G. E. Scuseria and M. Ernzerhof, Erratum: Hybrid functionals based on a screened Coulomb potential, [*J. Chem. Phys.*, 2003, **118**, 8207] *J. Chem. Phys.* 2006, **124**, 219906.

53 M. H. Du, Efficient carrier transport in halide perovskites: theoretical perspectives, *J. Mater. Chem. A*, 2014, **2**, 9091–9098.

54 P. Umari, E. Mosconi and F. De Angelis, Relativistic GW calculations on $CH_3NH_3PbI_3$ and $CH_3NH_3SnI_3$ perovskites for solar cell applications, *Sci. Rep.*, 2014, **4**, 4467.

55 C. Bernal and K. Yang, First-principles hybrid functional study of the organic–inorganic perovskites $CH_3NH_3SnBr_3$ and $CH_3NH_3SnI_3$, *J. Phys. Chem. C*, 2014, **118**, 24383–24388.

56 J. Im, C. C. Stoumpos, H. Jin, A. J. Freeman and M. G. Kanatzidis, Antagonism between Spin–Orbit Coupling and Steric Effects Causes Anomalous Band Gap Evolution in the Perovskite Photovoltaic Materials $CH_3NH_3Sn_{1-x}Pb_xI_3$, *J. Phys. Chem. Lett.*, 2015, **6**, 3503–3509.

57 J. Even, L. Pedesseau, J.-M. Jancu and C. Katan, DFT and k·p modelling of the phase transitions of lead and tin halide perovskites for photovoltaic cells, *Phys. Status Solidi RRL*, 2014, **8**, 31–35.

58 P. E. Blöchl, O. Jepsen and O. K. Andersen, Improved tetrahedron method for Brillouin-zone integrations, *Phys. Rev. B: Condens. Matter Mater. Phys.*, 1994, **49**, 16223.

5146 | *J. Mater. Chem. C*, 2019, **7**, 5139–5147

This journal is © The Royal Society of Chemistry 2019

59 M. Gajdoš, K. Hummer, G. Kresse, J. Furthmüller and F. Bechstedt, Linear Optical Properties in the Projector-Augmented Wave Methodology, *Phys. Rev. B: Condens. Matter Mater. Phys.*, 2006, **73**, 045112.

60 S. Baroni, S. De Gironcoli, A. Dal Corso and P. Giannozzi, Phonons and related crystal properties from density-functional perturbation theory, *Rev. Mod. Phys.*, 2001, **73**, 515.

61 R. Sanderson, *Chemical bonds and bonds energy*, Elsevier, 2012, vol. 21.

62 A. M. Ganose, C. N. Savory and D. O. Scanlon, $(CH_3NH_3)_2Pb(SCN)_2I_2$: A More Stable Structural Motif for Hybrid Halide Photovoltaics?, *J. Phys. Chem. Lett.*, 2015, **6**, 4594–4598.

63 J. Paier, M. Marsman and G. Kresse, Dielectric properties and excitons for extended systems from hybrid functionals, *Phys. Rev. B: Condens. Matter Mater. Phys.*, 2008, **78**, 121201.

64 A. E. Maughan, A. M. Ganose, M. M. Bordelon, E. M. Miller, D. O. Scanlon and J. R. Neilson, Defect Tolerance to Intolerance in the Vacancy-Ordered Double Perovskite Semiconductors Cs_2SnI_6 and Cs_2TeI_6, *J. Am. Chem. Soc.*, 2016, **138**, 8453–8464.

65 L. Yu and A. Zunger, Identification of potential photovoltaic absorbers based on first-principles spectroscopic screening of materials, *Phys. Rev. Lett.*, 2012, **108**, 068701.

66 T. Ishihara, Optical properties of PbI-based perovskite structures, *J. Lumin.*, 1994, **60**, 269–274.

67 J. Even, L. Pedesseau and C. Katan, Understanding quantum confinement of charge carriers in layered 2D hybrid perovskites, *ChemPhysChem*, 2014, **15**, 3733–3741.

68 A. Zakutayev, C. M. Caskey, A. N. Fioretti, D. S. Ginley, J. Vidal, V. Stevanovic, E. Tea and S. Lany, Defect Tolerant Semiconductors for Solar Energy Conversion, *J. Phys. Chem. Lett.*, 2014, **5**, 1117–1125.

69 A. M. Ganose, A. J. Jackson and D. O. Scanlon, sumo: Command-line tools for plotting and analysis of periodic ab initio calculations, *Journal of Open Source Software*, 2018, **3**, 717.

This journal is © The Royal Society of Chemistry 2019

J. Mater. Chem. C, 2019, **7**, 5139–5147 | **5147**